



Wet Chemical Synthesis of $Sb_4O_5Cl_2$ Used as an Effective Photocatalyst for Methylene Blue and Crystal Violet Degradation under Visible Light Irradiation

Rachid Makhloufi^{1*}, Salah Eddine Hachani², Asma Fettah³, Bahia Messai¹

¹Laboratory of Applied Chemistry (LCA), University of Biskra, P.O. Box 145, Biskra 07000, Algeria

²Department of Process Engineering & Petrochemistry, Faculty of Technology, University of El Oued, P.O. Box 789, El-Oued 39000, Algeria

³Laboratory of Molecular Chemistry and Environment, University of Biskra, P.O. Box 145, Biskra 07000, Algeria

Corresponding Author Email: r.makhloufi@univ-biskra.dz

<https://doi.org/10.18280/acsm.460202>

ABSTRACT

Received: 3 February 2022

Accepted: 5 April 2022

Keywords:

antimony oxychloride $Sb_4O_5Cl_2$, wet chemistry synthesis, methylene blue dye, crystal violet dye, photocatalytic degradation

The present scientific contribution aims to elaborate antimony oxychloride $Sb_4O_5Cl_2$ via a wet chemistry method and to study its photocatalytic activity to degrade methylene blue and crystal violet cationic dyes. The prepared samples were characterized using powder X-ray diffraction PXRD, Fourier transform infrared spectroscopy FTIR, Scanning electron microscopy analysis SEM and UV-Visible measurements. PXRD results revealed that the $Sb_4O_5Cl_2$ was successfully formed in a monoclinic phase structure with $P2_1/a$ space group. FTIR results show the presence of all characteristic bands that distinguished the prepared compound mainly include Sb–O, Sb–O–Sb, and Sb=O vibrating modes bands located at 503, 607, and 832 cm^{-1} , respectively. SEM micrograph showed that the microstructure of the prepared antimony oxychloride is composed of particles with sand rose morphology. UV-Visible outcomes demonstrated that our synthesized $Sb_4O_5Cl_2$ is an efficient photocatalyst for the degradation of both methylene blue MB and crystal violet CV targeted dyes. MB degradation reached 93.67% after 30 min while CV degradation up to 92.56% after 360 min.

1. INTRODUCTION

Organic dyes are largely and massively used for their high ability to absorb light in many daily life sectors such as textile, food processing, paper, painting, cosmetics, pharmaceuticals, and so on [1]. Organic dyes effluents became a serious problem because of their significant negative impact on both human health and its surrounded environment including water, soil and climate [2].

Methylene blue MB (Figure 1.a) dye is a heterocyclic aromatic chemical compound with the chemical formula of $C_{16}H_{18}N_3S^+Cl^-$. This cationic dye is used in medicine as a treatment for methemoglobinemia, burn care and urinary tract infections, biology as a staining agent, radiology, textile [3, 4]. However, methylene blue may cause hemolytic anemia, respiratory distress, pulmonary edema, photo-toxicity and bluish discoloration of tracheal secretions and urine [5].

Crystal violet CV (Figure 1.b) with chemical formula $C_{25}N_3H_{30}Cl$ is an organic dye used in Gram's Method of classifying different bacteria, textile, pharmaceutical, paints and printing ink [6]. However, human body contamination by crystal violet dye can lead to respiratory problems, renal insufficiency, corneal and conjunctiva irritation, skin diseases and in even cases cancers. CV effluents discharging can alter the aquatic system and marine life due to its mutagenic, teratogenic and mitotic poisoning nature [7].

For dye removal, a variety of technological techniques have been employed, including ion-floatation, coagulation, degradation, sedimentation, and adsorption [8, 9]. These approaches are efficient and applicable at industrial scale.

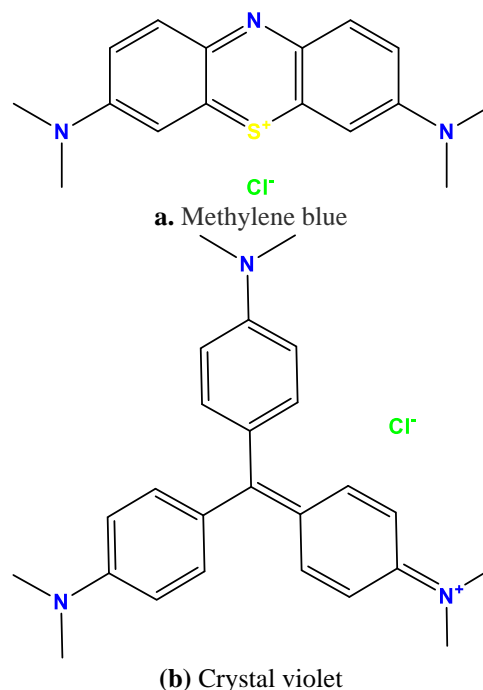


Figure 1. Molecular structures

However, they exhibit various disadvantages like time consuming, high-cost complexity, etc. Semiconductor based photocatalysis leads to a heterogeneous photochemical catalytic reaction on the surface of a solid semiconductor

driving to degrade the targeted dye [10]. This technique is much recommended for water treatment thanks to its simplicity, low cost and the lack of secondary pollution metabolites [11].

Antimony oxychloride $\text{Sb}_4\text{O}_5\text{Cl}_2$ is a semiconductor material with a direct band-gap of 3.12-3.38 eV. This material crystallizes in a monoclinic phase structure with the $\text{P}2_1/\text{a}$ space group under ordinary conditions [12-14]. According to the literature, the structure of antimony oxychloride is made up of layers containing antimony oxide units of which the chlorine ions occupy the free volume between the adjacent layers $(\text{Sb}_4\text{O}_5^{2+})_n$ as exhibited in Figure 2. In fact, the asymmetric part of the unit cell of $\text{Sb}_4\text{O}_5\text{Cl}_2$ contains two Sb atoms with different coordination. The first can be regarded as either three- or four-coordinated by O. The second, however, has only three O atoms in the coordination polyhedron and the next nearest neighbor is a Cl^- ion [14]. $\text{Sb}_4\text{O}_5\text{Cl}_2$ is used as flame retardant, optics, lithium and chloride storage materials [15, 16].

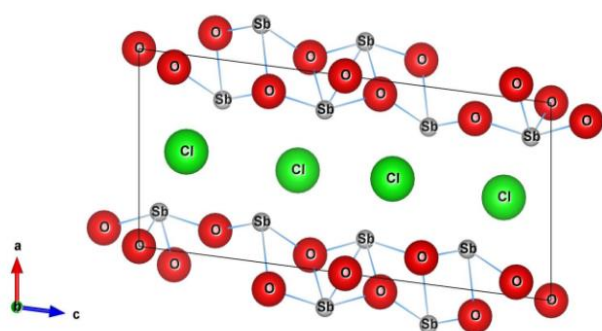


Figure 2. Crystal structure of antimony oxychloride $\text{Sb}_4\text{O}_5\text{Cl}_2$ (Projection onto [010] direction using VESTA version 3.5.0 program package)

According to the previous reports, antimony oxychloride $\text{Sb}_4\text{O}_5\text{Cl}_2$ can be elaborated using different techniques such as a hydrothermal route, template-free assembly method [17, 18]. Wet chemistry synthesis is an elaboration technique used to produce a desirable size and shape of metal oxides or sulfides particles. In this process, control over size and shape can be achieved by a better understanding of elementary events related to the reagents, the precursor conversion mechanism, surface stabilizing agent and growth and nucleation rate [19].

To the best of our knowledge, there is no published scientific report treating the utility of using antimony oxychloride $\text{Sb}_4\text{O}_5\text{Cl}_2$ as a photocatalyst to degrade methylene blue MB and crystal violet CV model dyes. The present research focuses on synthesizing antimony oxychloride $\text{Sb}_4\text{O}_5\text{Cl}_2$ using wet chemistry process and investigate its photocatalytic activity to degrade methylene blue and crystal violet dyes. The obtained samples have been examined using PXRD and SEM analyses. UV-Visible measurements have been performed to assess the photocatalytic properties of the obtained material to get rid of the selected dyes from water.

2. EXPERIMENTAL

2.1 Samples elaboration

$\text{Sb}_4\text{O}_5\text{Cl}_2$ samples have been elaborated by a wet chemistry process without using any surfactant. Weight of antimony

trichloride SbCl_3 (BIOCHEM; purity +99%) powder was dissolved in 100 ml of distilled water. Sodium thiosulfate $\text{Na}_2\text{S}_2\text{O}_3$ (PROLABO; purity 99%) was introduced in the resulted aqueous solution as a complexing agent during the hydrolysis of antimony trichloride SbCl_3 . The resulting precursor was magnetically stirred for 10 hours at 90°C as described in the literature to obtain the required phase [20]. After this time, the obtained solid material was filtered, well washed with distilled water, and then dried in a laboratory oven at 100°C for a few hours.

2.2 Samples characterization

2.2.1 PXRD analysis

The phase identification of the prepared sample has been investigated by powder X-ray diffraction (PXRD) analysis. This test was performed employing a Bruker D8 Advanced diffractometer using a $\text{Cu K}\alpha$ X-ray source ($\lambda=1.5418 \text{ \AA}$) operating at 40 kV and 20 mA. Bragg angle scans were recorded from 10 to 80° .

2.2.2 FTIR spectroscopy analysis

Fourier transform infrared (FTIR) analysis has been carried out using a Shimadzu 8400s spectrophotometer. A small weight of the prepared sample was mixed with KBr powder and pressed to get a transparent sample. The spectrum of the sample under investigation was obtained within wavenumber ranging from 400 to 1300 cm^{-1} .

2.2.3 SEM analysis

Scanning electron microscopy (SEM) analysis was used to examine the morphology of the sample under investigation. The experiment was carried out employing TESCAN VEGA3 laboratory equipment operating at 20 kV under a high vacuum.

2.2.4 Photocatalytic activity test

UV-Vis spectra were periodically recorded to monitor changes in the concentration of each examined dye. The absorbance A_i obtained after stirring for 1 hour in the dark was considered to determine the solution's starting concentration C_i . After various periods of light exposure, the absorbance A_f was measured to estimate the residual concentration C_f . The degradation efficiency (DE) for every organic dye was computed using the equation below [21-23]:

$$DE (\%) = \frac{A_i - A_f}{A_i} \times 100 \quad (1)$$

3. RESULTS AND DISCUSSION

3.1 PXRD results

Powder X-rays diffraction experiment was carried out for phase identification. The search-match function of the Crystal Impact Match program package was used to compare the PXRD peaks in the diffractogram corresponding to the obtained sample to those in the ICDD-PDF database, as shown in Figure 3. It can be seen that the PXRD signals corresponding to the sample under probe well matched those of the $\text{Sb}_4\text{O}_5\text{Cl}_2$ phase (ICDD-PDF file No. 00-030-0091). The diffraction lines at $2\theta = 14.30^\circ, 21.83^\circ, 27.14^\circ, 28.61^\circ, 35.07^\circ,$ and 44.18° are assigned to (001), (210), (211), (-401), (-212), and (610) planes of $\text{Sb}_4\text{O}_5\text{Cl}_2$ monoclinic phase having space group $\text{P}2_1/\text{a}$ [14, 24]. No secondary phase has been detected.

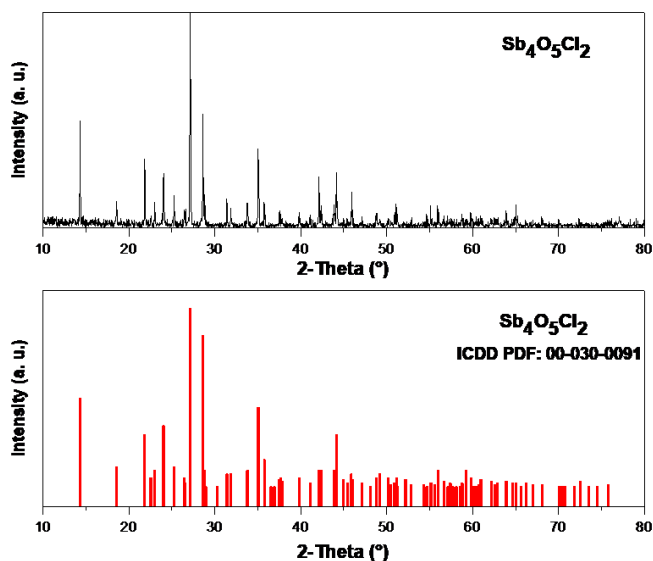


Figure 3. Comparison of PXRD pattern of the prepared sample with the ICDD-PDF database

Unit cell refinement from powder diffraction data has been performed using WinPLOTR version 2018 program package. The obtained cell lattice parameters and unit-cell volume are listed in Table 1. The calculated parameters related to the prepared $\text{Sb}_4\text{O}_5\text{Cl}_2$ monoclinic phase are very close to those of the ICDD-PDF database (ICDD-PDF file No. 00-030-0091).

Table 1. The obtained lattice parameters (a , b , c , α , β and γ) and unit-cell volume (V) of the studied crystalline system

a (Å)	6.229 (2)
b (Å)	5.107 (2)
c (Å)	13.500 (5)
α (°)	90.000
β (°)	97.270 (2)
γ (°)	90.000
V (Å ³)	426.003

3.2 FTIR results

The FTIR spectrum of the synthesized $\text{Sb}_4\text{O}_5\text{Cl}_2$ is shown in Figure 4. As can be seen, there are strong bands at 503 and 832 cm^{-1} , these bands are assigned to a single bond Sb–O and a double bond Sb=O vibrating modes, respectively. The absorption band located at 607 cm^{-1} is attributed to the symmetric Sb–O–Sb vibrating mode and the band observed at 712 cm^{-1} is dedicated to an asymmetric Sb–O–Sb vibrating mode. Our experimental findings are in full agreement with the results earlier reported in the literature [25]. Besides, no chloride bond peak has been appeared, indicating that Cl⁻ anions don't form any bonds in the structure and just occupy the free volume between the antimony oxide layers as described in the introduction part.

3.3 SEM results

The morphology of an elaborated material is an important parameter influencing the resulting properties including mechanical modulus, heat transfer constant, dielectric constant and catalytic properties. Scanning electron microscopy was used to investigate the morphology of the prepared samples. Figure 5 illustrates the SEM micrograph of the elaborated

sample. It is clear to observe that the microstructure corresponding to antimony oxychloride $\text{Sb}_4\text{O}_5\text{Cl}_2$ prepared by a wet chemistry route is composed of particles with sand rose morphology.

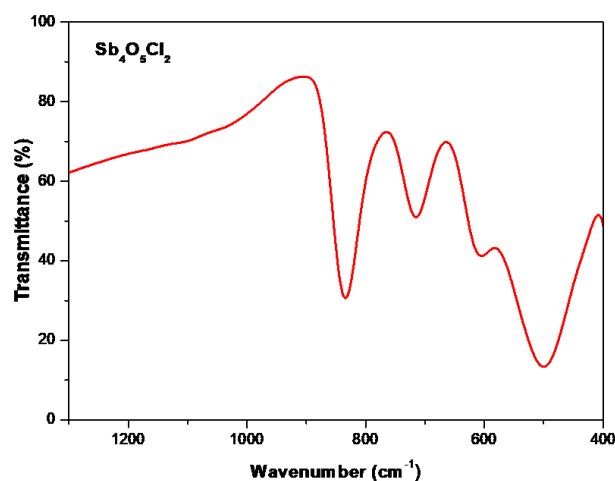


Figure 4. FTIR spectrum of the prepared $\text{Sb}_4\text{O}_5\text{Cl}_2$ by wet chemistry

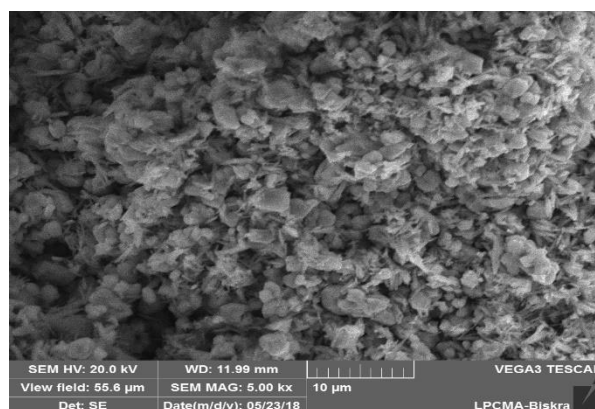


Figure 5. SEM micrograph of the prepared $\text{Sb}_4\text{O}_5\text{Cl}_2$ by wet chemistry

3.4 Photocatalytic activity of the prepared antimony oxychloride

The photocatalytic properties of the obtained antimony oxychloride $\text{Sb}_4\text{O}_5\text{Cl}_2$ were studied via the degradation of methylene blue MB and crystal violet CV as targeted dyes. Analytical samples of MB and CV solutions containing the prepared material were exposed to visible light irradiation. Figure 6 illustrates the change in MB dye absorption as a function of time exposed to visible light irradiation. It is evident that the absorbance at the main band of MB decreased from 1.863 to 0.118 after 30 min of light exposure indicating that this dye was photodegraded in the presence of $\text{Sb}_4\text{O}_5\text{Cl}_2$ as photocatalyst which is experimentally proved by the rapid transformation of MB typical color from blue to transparent when exposed to visible light irradiation for different time intervals. We report a similar tendency in the case of CV dye where the absorbance was also found to decrease from 1.263 to 0.094 after 360 min as presented in Figure 7 revealing that CV dye was photodegraded in the presence of $\text{Sb}_4\text{O}_5\text{Cl}_2$ but in a longer exposure time to light illumination compared to MB dye.

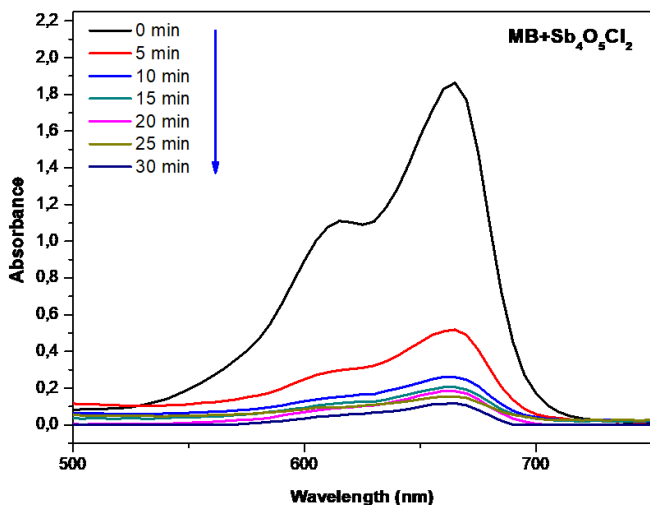


Figure 6. UV-Visible spectra of photodegraded methylene blue in the presence of $\text{Sb}_4\text{O}_5\text{Cl}_2$ under visible light irradiation

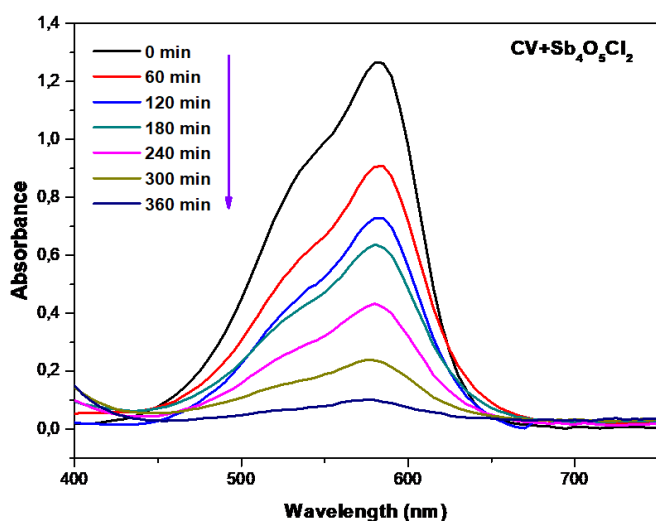


Figure 7. UV-Visible spectra of photodegraded crystal violet in the presence of $\text{Sb}_4\text{O}_5\text{Cl}_2$ under visible light irradiation

Figure 8 shows the time-dependent evolution of methylene blue MB degradation efficiency in the presence of $\text{Sb}_4\text{O}_5\text{Cl}_2$ photocatalyst under visible light exposure. It can be shown that the removal efficiency of MB rapidly increased with the time of visible light illumination. The removal efficiency of MB reached 93.67% after 30 min. However, the time dependence of the degradation efficacy of CV dye in the presence of $\text{Sb}_4\text{O}_5\text{Cl}_2$ is shown in Figure 9. The degradation efficacy of CV dye increased with the increment of exposure time to visible light illumination, this photocatalytic parameter up to 92.56% after 360 min of exposure time. Our results are better than those reported by Guo et al. and Mahanta et al. who studied the MB dye photocatalytic degradation in the presence of BiVO_4 [26] and $\text{TiO}_2\text{-SiO}_2$ nanoparticles [27], respectively, as photocatalysts. Neena and coworkers have reported less removal efficiency of MB dye using nanosized novel Fe-Cd co-modified ZnO as a photocatalyst [28] compared to our outcomes. In a recent study, Kossar et al. found that when exposed to visible light irradiation, bismuth ferrite nanoparticles degrade 84.5 percent toward CV dye [29]. This removal proportion is less than that reported in our study.

The device simplicity and the fast time of degradation process in the presence of $\text{Sb}_4\text{O}_5\text{Cl}_2$ particles as a photocatalyst as well as the higher reported removal efficiencies of the targeted dyes that generating harmless degradation products allowing say that the photocatalysis is a successful, rapid, efficient, eco-friendly, and very recommended method to remove organic dyes from waste water.

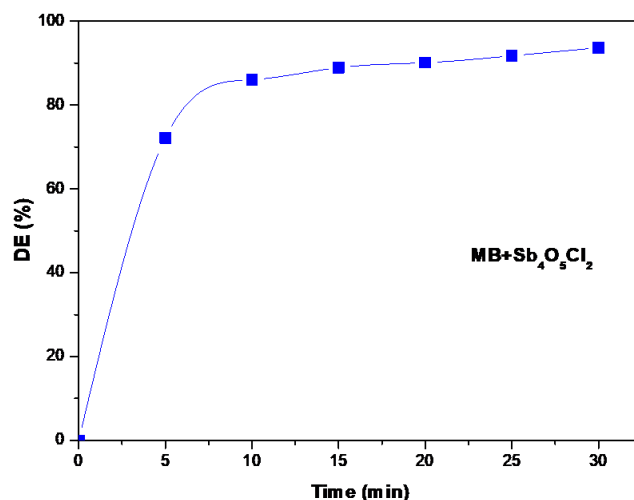


Figure 8. The evolution of degradation efficiency of methylene blue MB as a function of time exposure to light illumination

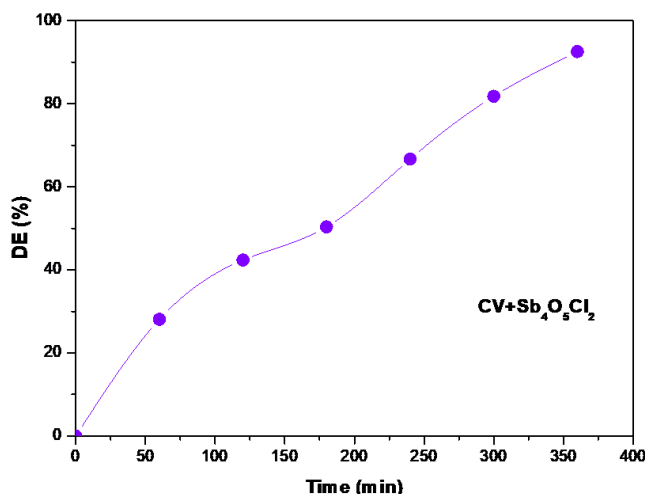


Figure 9. The progression of degradation efficiency of crystal violet CV as a function of time exposure to light illumination

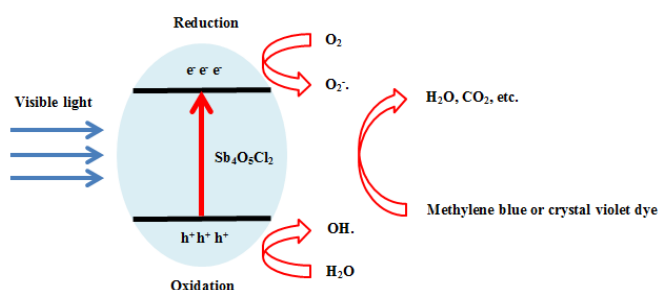


Figure 10. Reactive scheme describing MB and CV degradation in the presence of $\text{Sb}_4\text{O}_5\text{Cl}_2$ under light visible irradiation

3.4.1 Photodegradation mechanism

When $\text{Sb}_4\text{O}_5\text{Cl}_2$ semiconductor particles were subjected to a visible light beam having an energy ($h\nu$) larger than their direct band-gap, electron-hole pairs would be formed. A certain number of these photo-induced pairs recombined while others transferred onto the surface of $\text{Sb}_4\text{O}_5\text{Cl}_2$ and then reacted with adsorbed oxygen/ H_2O to give $\text{O}_2^{\cdot-}$ and H_2O_2 . However, hydroxyl radical OH^{\cdot} can be produced either by the reaction of photo-generated holes with water molecules or by the reaction of $\text{O}_2^{\cdot-}$ with H_2O_2 . The reactive chemical species including $\text{O}_2^{\cdot-}$, H_2O_2 and OH^{\cdot} could degrade the organic dye into H_2O , CO_2 and other products [30]. The possible mechanism describing the degradation of the selected dyes in the presence of $\text{Sb}_4\text{O}_5\text{Cl}_2$ as photocatalyst is supposed as following (Figure 10).

4. CONCLUSIONS

We have successfully synthesized antimony oxychloride $\text{Sb}_4\text{O}_5\text{Cl}_2$ and evaluated the feasibility of using this semiconductor material as a photocatalyst to eliminate methylene blue and crystal violet contaminants from water. Based on the above considerations, we can assume that:

- PXRD results revealed that a pure $\text{Sb}_4\text{O}_5\text{Cl}_2$ monoclinic phase has been successfully elaborated.
- FTIR results declared the presence of typical vibrating bands related to $\text{Sb}_4\text{O}_5\text{Cl}_2$ monoclinic phase principally Sb–O, asymmetric Sb–O–Sb, and Sb=O vibrating modes bands located at 503, 712, and 830 cm^{-1} , respectively, with the absence of any chloride bond peak which confirms the layered structure of the prepared antimony oxychloride as mentioned in the introduction section.
- SEM images demonstrated that the microstructure of the prepared material is formed by microparticles with sand rose morphology.
- According to UV-visible analysis and absorbance measurements, the prepared antimony oxychloride can be employed as an efficient photocatalyst for the removal of both methylene blue and crystal violet dyes.
- After 30 minutes of visible light irradiation, the degradation efficiency of MB enhanced to 93.67 percent in the presence of $\text{Sb}_4\text{O}_5\text{Cl}_2$ as a photocatalyst.

After 360 minutes of visible light irradiation, the degradation efficiency of CV reaches 92.56 percent in the presence of $\text{Sb}_4\text{O}_5\text{Cl}_2$ as a photocatalyst.

REFERENCES

[1] Fröse, A., Schmidtke, K., Sukmann, T., Junger, I.J., Ehrmann, A. (2019). Application of natural dyes on diverse textile materials. *Optik*, 181: 215-219. <https://doi.org/10.1016/j.ijleo.2018.12.099>

[2] Lellis, B., Fávaro-Polonio, C.Z., Pamphile, J.A., Polonio, J.C. (2019). Effects of textile dyes on health and the environment and bioremediation potential of living organisms. *Biotechnology Research and Innovation*, 3(2): 275-290. <https://doi.org/10.1016/j.biori.2019.09.001>

[3] Nedu, M.E., Tertis, M., Cristea, C., Georgescu, A.V. (2020). Comparative Study Regarding the Properties of

methylene blue and proflavine and their optimal concentrations for in vitro and in vivo applications. *Diagnostics*, 10(4): 223. <https://doi.org/10.3390/diagnostics10040223>

[4] Church, J.T., Posluszny, J.A., Hemmila, M., To, K.B., Cherry-Bukowiec, J.R., Waljee, J. (2015). Methylene blue for burn-induced vasoplegia: Case report and review of literature. *Journal of Burn Care & Research*, 36: e107-e111. <https://doi.org/10.1097/BCR.000000000000134>

[5] Ginimuge, P.R., Jyothi, S. (2010). Methylene blue: Revisited. *Journal of Anaesthesiology, Clinical Pharmacology*, 26(4): 517-520.

[6] Mani, S., Bharagava, R.N. (2016). Exposure to crystal violet, its toxic, genotoxic and carcinogenic effects on environment and its degradation and detoxification for environmental safety. *Reviews of Environmental Contamination and Toxicology*, 237: 71-104. https://doi.org/10.1007/978-3-319-23573-8_4

[7] Nasiri, S., Alizadeh, N. (2019). Synthesis and adsorption behavior of hydroxypropyl- β -cyclodextrin-polyurethane magnetic nanoconjugates for crystal and methyl violet dyes removal from aqueous solutions. *RSC Advances*, 42: 24603-24616. <https://doi.org/10.1039/C9RA03335A>

[8] Gadekar, M.R., Ahammed, M.M. (2020). Use of water treatment residuals for colour removal from real textile dye wastewater. *Applied Water Science*, 10: 1-8. <https://doi.org/10.1007/s13201-020-01245-9>

[9] Rafiq, A., Ikram, M., Ali, S., Niaz, F., Khan, M., Khan, Q., Maqbool, M. (2021). Photocatalytic degradation of dyes using semiconductor photocatalysts to clean industrial water pollution. *Journal of Industrial and Engineering Chemistry*, 97: 111-128. <https://doi.org/10.1016/j.jiec.2021.02.017>

[10] Thongam, D.D., Chaturvedi, H. (2021). Advances in nanomaterials for heterogeneous photocatalysis. *Nano Express*, 2(1): 012005. <https://doi.org/10.1088/2632-959X/abeb8d>

[11] Han, G., Chen, D., Li, X. (2017). Synthesis and catalytic performance of antimony trioxide nanoparticles by ultrasonic-assisted solid-liquid reaction ball milling. *Advances Powder Technology*, 28(4): 1136-1140. <https://doi.org/10.1016/j.appt.2017.01.019>

[12] Liu, Y., Yuan, X., Wang, H., Chen, X., Gu, S., Jiang, Q., Wu, Z., Jiang, L., Wu, Y., Zeng, G. (2015). Novel visible light-induced g-C₃N₄-Sb₂S₃/Sb₄O₅Cl₂ composite photocatalysts for efficient degradation of methyl orange. *Catalysis Communications*, 70: 17-20. <https://doi.org/10.1016/j.catcom.2015.07.015>

[13] Edstrand, M. (1947). On the crystal structure of the antimony oxychloride $\text{Sb}_4\text{O}_5\text{Cl}_2$ and isomorphous oxybromide. *Acta Chemica Scandinavica*, 1: 178-203. <https://doi.org/10.3891/acta.chem.scand.01-0178>

[14] Särnstrand, C. (1978). The crystal structure of antimony(III) chloride oxide $\text{Sb}_4\text{O}_5\text{Cl}_2$. *Acta Crystallogr., Sect. B: Struct. Sci., Cryst. Eng. Mater.*, 34: 2402-2407. <https://doi.org/10.1107/S056774087800833X>

[15] Lv, S.Y., Chen, Y.X., Li, X.H., Luo, W.F., Wang, Y.M., Xu, W.X., Qyyum, A., Zhang, H. (2020). $\text{Sb}_4\text{O}_5\text{Cl}_2$ for 34th-order-harmonic mode locking. *Optical Materials*, 100: 109635. <https://doi.org/10.1016/j.optmat.2019.109635>

[16] Hu, X., Chen, F., Wang, S., Ru, Q., Chu, B., Wei, C., Shi, Y., Ye, Z., Chu, Y., Hou, X., Sun, L. (2019). Electrochemical performance of $\text{Sb}_4\text{O}_5\text{Cl}_2$ as a new

- anode material in aqueous chloride-ion battery. *ACS Appl. Mater. Interfaces* 11: 9144-9148. <https://doi.org/10.1021/acsami.8b21652>
- [17] Chen, X.Y., Huh, X.Y., Lee, S.W. (2008). Hydrothermal synthesis of antimony oxychloride and oxide nanocrystals: $Sb_4O_5Cl_2$, $Sb_8O_{11}Cl_2$, and Sb_2O_3 . *Journal of Solid State Chemistry*, 181(9): 2127-2132. <https://doi.org/10.1016/j.jssc.2008.04.043>
- [18] Yang, L., Huang, J., Cao, L., Shi, L., Yu, Q., Kong, X., Jie, Y. (2016). pH-regulated template-free assembly of $Sb_4O_5Cl_2$ hollow microsphere crystallites with self-narrowed bandgap and optimized photocatalytic performance. *Scientific Report*, 6: 1-11. <https://doi.org/10.1038/srep27765>
- [19] Raudoniene, J., Skaudzius, R., Zarkov, A., Selskis, A., Karlsson, O., Kareiva, A., Garskaite, E. (2019). Wet-chemistry synthesis of shape-controlled Ag_3PO_4 crystals and their 3D surface reconstruction from SEM imagery. *Powder Technology*, 345: 26-34. <https://doi.org/10.1016/j.powtec.2018.12.091>
- [20] Gusatti, M., Barroso, G.S., de Campos, C.E.M., de Souza, D.A.R., de Almeida Rosário, J., Lima, R.B., Milioli, C.C., Silva, L.A., Riella, H.G., Kuhnen, N.C. (2011). Effect of different precursors in the chemical synthesis of ZnO nanocrystals. *Mater. Res.*, 14(2): 264-267. <https://doi.org/10.1590/S1516-14392011005000035>
- [21] Abdellah, M.H., Nosier, S.A., El-Shazly, A.H., Mubarak, A.A. (2018). Photocatalytic decolorization of methylene blue using TiO_2/UV system enhanced by air sparging. *Alexandria Engineering Journal*, 57(4): 3727-3735. <https://doi.org/10.1016/j.aej.2018.07.018>
- [22] Rahmat, M., Rehman, A., Rahmat, S., Bhatti, H.N., Iqbal, M., Khan, W.S., Bajwa, S.Z., Rahmat, R., Nazir, A. (2019). Highly efficient removal of crystal violet dye from water by MnO_2 based nanofibrous mesh/photocatalytic process. *Journal of Materials Research and Technology*, 8(6): 5149-5159. <https://doi.org/10.1016/j.jmrt.2019.08.038>
- [23] Chen, L., Tran, T., Huang, C., Li, J., Yuan, L., Cai, Q. (2013). Synthesis and photocatalytic application of Au/Ag nanoparticle-sensitized ZnO films. *Applied Surface Science*, 273: 82-88. <https://doi.org/10.1016/j.apsusc.2013.01.184>
- [24] Huang, L., Zhang, L., Bao, D., Jiang, X., Li, J., Sun, X. (2020). Ultrasound-assisted synthesis of $rGO/Sb_4O_5Cl_2/Sb_2S_3$ for a high photo-catalytic rate. *New Journal of Chemistry*, 44: 3103-3111. <https://doi.org/10.1039/C9NJ05830C>
- [25] Li, Q., Liu, Z., Guo, X., Huang, K., Xu, S., Zhang, D., Itagaki, K. (2000). Template Effect of Some Ions on the Structures and Morphologies of $Ni(OH)_2$ and Sb_2O_3 . *Shigen-to-Sozai* 116(8): 698-702. <https://doi.org/10.2473/shigentosozai.116.698>
- [26] Guo, Y., Yang, X., Ma, F., Li, K., Xu, L., Yuan, X., Guo, Y. (2010). Additive-free controllable fabrication of bismuth vanadates and their photocatalytic activity toward dye degradation. *Applied Surface Science*, 256(7): 2215-2222. <https://doi.org/10.1016/j.apsusc.2009.09.076>
- [27] Mahanta, U., Khandelwal, M., Deshpande, A.S. (2022). $TiO_2@SiO_2$ nanoparticles for methylene blue removal and photocatalytic degradation under natural sunlight and low-power UV light. *Applied Surface Science*, 576: 151745. <https://doi.org/10.1016/j.apsusc.2021.151745>
- [28] Neena, D., Kondamareddy, K.K., Bin, H., Lu, D., Kumar, P., Dwivedi, R.K., Pelenovich, V.O., Zhao, X.Z., Gao, W., Fu, D. (2018). Enhanced visible light photodegradation activity of RhB/MB from aqueous solution using nanosized novel Fe-Cd co-modified ZnO. *Scientific Reports*, 8: 1-12. <https://doi.org/10.1038/s41598-018-29025-1>
- [29] Kossar, S., Banu, I.B., Aman, N., Amiruddin, R. (2021). Investigation on photocatalytic degradation of crystal violet dye using bismuth ferrite nanoparticles. *Journal of Dispersion Science and Technology*, 42(14): 2053-2062 (2021). <https://doi.org/10.1080/01932691.2020.1806861>
- [30] Zhang, R., Cui, H., Yang, X., Tang, H., Liu, H., Li, Y. (2012). Facile hydrothermal synthesis and photocatalytic activity of rod-like nanosized silver tungstate. *Micro Nano Lett.*, 7: 1285-1288. <https://doi.org/10.1049/mnl.2012.0765>